Targeting the Pentose Phosphate Pathway: Characterization of a New 6PGL Inhibitor

Anh Tuan T Tran, Aude Sadet, Paolo Calligari, Philippe Lopes, Jamal Ouazzani, Matthieu Sollogoub, Emeric Miclet, Daniel Abergel

Targetting the Pentose Phosphate Pathway: characterization of a new 6PGL inhibitor

A.T. Tran, A. Sadet, P. Calligari, P. Lopes, J. Ouazzani, M. Sollogoub, E. Miclet and D. Abergel

February 22, 2018

Abstract

Human African trypanosomiasis, or sleeping sickness, is a lethal disease caused by the protozoan parasite *Trypanosoma brucei*. However, although many efforts have been made to understand the biochemistry of this parasite, drug development has led to treatments that are of limited efficiency and of great toxicity. In order to develop new drugs, new targets must be identified, and among the several metabolic processes of trypanosomes that have been proposed as drug targets, carbohydrate metabolism (glycolysis and the Pentose Phosphate Pathway-PPP) appears as a promising one. As far as the PPP is concerned, a limited number of studies are related to the glucose-6-phosphate dehydrogenase (G6PDH). In this work, we have focused on the activity of the second PPP enzyme (6PGL) that transforms 6-phosphogluconolactone into 6-phosphogluconic acid. A lactam analogue of the natural substrate has been synthesized and binding of the ligand to 6PGL has been investigated by NMR titration. The ability of this ligand to inhibit 6PGL has also been demonstrated using UV experiments, and protein-inhibitor interactions have been investigated through docking calculations and molecular dynamics simulations. In addition, a marginal inhibition of the third enzyme of the PPP (6-phosphogluconate dehydrogenase) was also demonstrated. Our results thus open new prospects for targetting *T. brucei*.

Abbreviations

- 6PGL: 6-phosphogluconolactonase
- 6-PGA: 6-phosphogluconic acid
- G-6-P: Glucose-6-phosphate
- 6PGDH: 6-phosphogluconate dehydrogenase
- G6PDH: Glucose-6-phosphate dehydrogenase
- NADPH: Nicotinamide Adenine Dinucleotide Phosphate

Introduction

Human African trypanosomiasis, or sleeping sickness, is a lethal disease caused by the protozoan parasite *Trypanosoma brucei*.[1, 2] The parasite is transmitted to the human host through the bite of the Tse-Tse fly. Despite a significant reduction in the disease prevalence

over the past 15 years, the sleeping sickness is still endemic in rural parts of sub-Saharan African countries with 3,000 new infections annually.[3] These parasites have been the object of many studies in the recent decades, and great progress have been made in the understanding of their biochemistry. However, these efforts have led to the development of treatments that are of limited efficiency and of great toxicity. Therefore, in order to develop new drugs, it is important to identify new targets, and a natural way to achieve this goal is to focus on specific metabolic pathways. Several metabolic processes of trypanosomes have been proposed as drug targets. Among these, carbohydrate metabolism appears as a promising one. This was motivated by the fact that Trypanosomes contain a separate intracellular compartment, the glycosome, where the first seven steps of glycolysis, and the first three steps of the pentose phosphate pathway (PPP) take place.[4, 5] This unusual location of such major pathways inside a specific organelle has endowed the parasitic enzymes with physicochemical properties that are different from those of their human counterparts, which are located in the cytosol. This may be exploited in a drug design process. In this drug development perspective, glycolysis has been investigated, and several of its enzymes have been identified as potentially good targets.[6, 7] The focus on glycolysis has been supported by a series of studies, one of which has shown that a 50% reduction in ATP production in *T. brucei* leads to the parasite death (see [8] for a review).

The PPP has also been recognized as an attractive drug target,[9] and several pieces of work have focused on glucose-6-phosphate dehydrogenase (G6PDH), one of its key enzyme. However, only a limited number of studies are available on enzymes of the PPP, for parasites and for mammalian homologues,[10] although this pathway is of particular importance. Indeed, PPP produces NADPH, which serves as a hydrogen donor in various biosynthetic processes, and has an important role in case of oxidative attack by the infected host. Besides, 3D structures of the second and third PPP enzymes of *T. brucei*, the 6-phospho-gluconolactonase (6PGL) and the 6-phosphogluconate dehydrogenase (6PGDH) have been solved.[11, 12] This is of particular interest, as structural differences between the parasitic and mammalian 6PGDH have been exploited to design molecules that would be specific inhibitors of the *T. brucei* enzyme.[13]

In this work, we present what is, to our knowledge, the first inhibitor of the protein 6PGL. This inhibitor, conceived as an analogue of the 6PGL substrate, was shown to bind the active site of the protein in place of the δ-phosphogluconolactone. Binding affinity was characterized by Nuclear Magnetic Resonance (NMR), and enzyme inhibition was studied by reaction rate measurements of the enzymatic activities through UV absorption. Moreover, *in silico* studies based on docking and Molecular Dynamics (MD) simulations allowed to shed light on the interaction mechanism between 6PGL and its inhibitor.

Materials and Methods

Chemical synthesis

The characterization of the various compounds in the synthesis of GP269 relied on ^{1}H and ^{13}C NMR spectroscopy, as well as Electrospray-ionization High-resolution mass spectroscopy (ESI-HRMS). Details are given in SI. An overview of the chemical synthesis and chemical formulas of the various intermediates and of the final product are depicted in Fig. 1.

Compound 3

To a solution of compound **2** (13 g, 18 mmol) in acetone (250 mL) at 0^o C was added NBS (3.8 g, 21 mmol). The mixture was stirred at room temperature for 30 min. The reaction was quenched dropwise with $NaHCO_3$ at 0^o C and the acetone was removed under reduced pressure. DCM was added to the residue and the organic layer was washed with sat. $Na_2S_2O_3$, water, dried over $MgSO_4$, filtered and concentrated. The residue was purified by chromatography on a short column (cyclohexane/EtOAc:86/14) to afford 6.55 g (60%) of hemiacetal **3** as a yellow oil.

Compound 4

Acetic anhydride (11.2 mL, 118.6 mmol) was added under an argon atmosphere to a solution of compound **3** (3.6 g, 5.93 mmol) in anhydrous DMSO (16.8 mL). The mixture was stirred at room temperature for 18h. The reaction mixture was diluted with Et_2O, washed with water, a 10% aq. $NaHCO_3$ solution and saturated brine. The organic layer was dried, filtered, concentrated, and purified by column chromatography (cyclohexane/EtOAc: 9/1) to give **4** (2.9 g, 81%) as a yellow oil. $[\alpha]_D^{23} = 41.5^o$ (c = 0.9, $CHCl_3$).

Compound 5

Compound **4** (820 mg, 1.35 mmol) was treated with NH_3 (2M in anhydrous methanol, 20 mL) at 0^o C for 1h. The reaction mixture was evaporated, co-evaporated three times with toluene to give compound **5** as yellow oil (96%). The structure of this intermediate was quickly analyzed and confirmed by ^{1}H NMR and ^{13}C NMR.

Compound 7

Acetic anhydride (2.4 mL, 25.8 mmol) was added under argon atmosphere to a solution of compound **6** (800 mg, 1.29 mmol) in anhydrous DMSO (3.7 mL). The mixture was stirred at room temperature for 24h. The reaction mixture was diluted with Et_2O, washed with water, a 10% aqueous $NaHCO_3$ solution and brine. The organic layer was dried, filtered and concentrated under reduced pressure to give compound **6** as a yellow oil.
Formic acid (2.45 mL, 65 mmol) was slowly added to a solution of $NaBH_3CN$ (138 mg, 2.2 mmol) and compound **6** in anhydrous acetonitrile. The reaction mixture was refluxed for 3h. After cooling to 0^o C, the mixture was quenched by addition of aqueous HCl (1M, 1.8 mL). After stirring for 15 min, the mixture was poured into a stirred (1/1) mixture of EtOAc/ aqueous $NaHCO_3$ (10%). The aqueous layer was extracted with EtOAc and then the organic layer was washed with brine, dried over $MgSO_4$, filtered, concentrated and purified by column chromatography with a 10% to 20% EtOAc in Cyclohexane gradients to give lactame **7** as a colorless oil (342 mg, 44%) over 2 steps. $[\alpha]_D^{23} = 85.0^o$ (c = 0.4, $CHCl_3$).

Compound 8

To a solution of **7** (260 mg, 0.43 mmol) in THF (12 mL), TBAF (1M in THF, 0.86 mL) was added. The mixture was stirred at room temperature for 2h. After completion, water was added and the mixture was extracted with DCM. The organic layer was dried over $MgSO_4$, evaporated under reduced pressure and purified by column chromatography (DCM/MeOH: 95/5) to give alcohol **8** (140 mg, 73%) as a white solid. $[\alpha]_D^{22} = 99.2$ (c = 1.1, $CHCl_3$); mp = 115^o C.

Compound 9

Dibenzyl N,N- diisopropyl phospharimidite (90%, 125 μL, 0.34 mmol) was added dropwise (30 min) under argon atmosphere to a solution of compound **12** (20 mg, 0.045 mmol) and tetrazole in acetonitrile (0.45M, 1.2 mL, 0.54 mmol). A suspension is observed. The reaction mixture was stirred at room temperature for 24 h. DCM (0.5 mL) was added and the mixture was cooled to -40^o C. A solution of MCPBA (150 mg, 0.87 mmol) in DCM was added dropwise and the mixture was left stirring at 0^o C for 3 h. The mixture was diluted with DCM and washed with a 10% aq. Na_2SO_3 solution, sat. $NaHCO_3$, water and brine. The organic phase was dried, concentrated and purified by column chromatography with a 20% to 50% EtOAc in cyclohexane gradients to give compound **14** as a pale yellow oil (20 mg, 65%) $[\alpha]_D^{22} = 60.0$ (c = 0.85, $CHCl_3$).

Compound 10: GP269

The $Pd(OH)_2/C$ (10 mg) was added to a solution of compound **14** (10 mg) in $MeOH/H_2O/THF$ (8:2:1) under argon atmosphere. Argon was removed under vacuo. The suspension was stirred under H_2 (balloon) for 48 h at room temperature. The mixture was filtered through celite and concentrated. The solid was lyophilized in H_2O to give desired lactam **10** as a white solid (3 mg, 73%).

NMR experiments

^1H-^{15}N HSQC experiments[14] were recorded on a Bruker Avance III spectrometer operating at a ^1H frequency of 500 MHz and equipped with a triple resonance, z-axis pulsed-field-gradient cryogenic probehead, optimized for ^1H detection. Spectra were acquired at 25°C, on a sample of 90 μM *Tb*6PGL, 20 mM KPO_4 pH 6.3, 120 mM NaCl, 11 μM DSS, 90% H_2O/10% D_2O. This sample was titrated with GP269 stock solutions of 35 mM or 5.3 mM GP269 in 50 mM KPO4 pH 6.3. Data were processed using TOPSPIN software using shifted sine-bell window functions and extensive zero-filling prior to Fourier transformation to yield high digital resolution.

For residues in fast exchange, the analysis of the variations of the chemical shift perturbations, $\Delta\delta$, upon titration was based on the following equation:[15]

$$\Delta\delta = \Delta\delta_{max}\frac{([P]_t + [L]_t + K_D) - \sqrt{([P]_t + [L]_t + K_D)^2 - 4[P]_t[L]_t}}{2[P]_t}, \quad (1)$$

where $[P]_t$ and $[L]_t$ are the total concentrations of protein and ligand, respectively, K_D is the dissociation constant of the GP269:6PGL complex, and $\Delta\delta_{max}$ is the maximum shift change on saturation, obtained from the HSQC spectrum with 10 Eq GP269. Data were fitted to Eq. 1 using a Levenberg-Marquardt algorithm, as implemented in the Origin® software.

Enzyme kinetics measurements

Sample preparation The reactive media for UV experiments were prepared from stock solutions with [Hepes] = 40 mM at pH = 7.5, [$NADP^+$] = 1 mM, [G-6-P] = 1 mM, and [6PGA] = 1 mM. Expression and purification of uniformly ^{15}N-labeled recombinant Tb6PGL were achieved as detailed in Ref. [16]. Purification yielded 6PGL dissolved in a solution containing [Hepes] = 50 mM at pH = 7, [NaCl] = 200 mM, and [DTT] = 1 mM. 6PGL was further diluted to reach a final concentration [6PGL] = 1.5 μg/mL.
The solution of yeast 6PGDH (Sigma-Aldrich) was prepared by dissolving 1.33 mg of dry protein into 200 μL of a Hepes Buffer with [Hepes] = 40 mM to reach a final concentration of

[6PGDH] = 18.2 μM, and pH was adjusted to 7.5 using a 1M NaOH solution. This amounts to $\approx$ 4.4 U/mL of 6PGDH activity, according to the supplier. Finally, G6PDH (NZytech) was purchased as a solution with 5 kU/mL.
For inhibition measurements, a stock solution with [GP269] = 20 mM was obtained by dissolving 4.5 mg of GP269 in 880 μL of D_2O. This stock solution was used to prepare additional solutions at various inhibitor concentrations.

Measurements of 6PGL activities UV assays were performed at 20^o C and carried out in duplicate on an Unicam UV 300 UV spectrophotometer. Measurements were performed on a 500 μL volume placed in a 1 cm optical path UV cell. Solutions contained 250 μM $NADP^+$, 10 U G6PDH and 0.3 U 6PGDH in a 10 mM Hepes buffer at pH= 7.5. Kinetic measurements were started at the time $t_0 = 1$ min where 50 μM G-6-P were added to the solution. Absorbance was measured at the maximum NADPH absorption wavelength ($\lambda = 340$ nm, $\epsilon_{340} = 6300$ L.mol^{-1}.cm^{-1} and at a rate of 4 points per second. A 10 μL volume of a 6PGL solution at 1.5 μg/mL was then added 2 minutes after the beginning of the G-6-P oxidation reaction, and Lactonase activity was monitored during the next 7 minutes at the same observation rate (4 measurements per second). Due to the manipulation of the sample outside of the spectrometer during this phase of the experiments, a number of data points are typically missing between times $t \approx 2'\ 40''$ and $t \approx 3'\ 20''$ (see Fig. 4).

Enzymatic oxidation of G-6-P by G6PDH is associated to the production of one NADPH equivalent, the reduced enzyme cofactor. Therefore, at complete G-6-P oxidation, one expects the UV absorbance curve to reach a plateau. However, this was not exactly the case, because of the subsequent spontaneous lactone hydrolysis. For this reason, and in order to determine the time of complete G-6-P oxidation, the NADPH production curve in the absence of 6PGL was fitted to an empirical bi-exponential function:

$$s(t) = A(2 - e^{-(t-t_0)/\tau_1} - e^{-(t-t_0)/\tau_2}). \tag{2}$$

In this expression, τ_1 and τ_2 are the signal build-up times and A corresponds to the maximum DO jump magnitude of both the first (G-6-P oxidation) and second (spontaneaous hydrolysis of the lactone) reactions. All fits were performed using the Scilab software.[17] 6PGL activity was indirectly assessed through the measurement of the absorbance of the NADPH produced by the following enzyme of the cascade (6PGDH). The slope of the linear portion of the UV signal corresponding to NADPH production by 6PGDH was determined by fitting experimental points to a straight line. In order to assess the accuracy of the slopes and the effect of contamination of the latter by erroneously including some nonlinear parts of the curve, computations were performed on various time intervals $[t_i, t_i + \Delta]$, with values

of $\Delta = 1$ and 3 min, and $t_i = 5, 5.5, 6, 6.5, 7, 7.5, 8$ min. Eventually, slopes were determined using measurements performed between times $t = 5$ and $t = 8$ min.

The approach used requires that 6PGDH activity be much larger than 6PGL activity, which ensures that the measured UV absorption curves reflect the sole 6PGL kinetics. This was assessed in the following way. Test experiments were first performed in a solution containing 6PGDH with an activity $A_{6\text{PGDH}} \approx 0.98$ U and various amounts of 6PGL, $m_{6PGL} = 150, 15, 0$ ng (see Table 1 in *Supplementary Information*). The dramatically different NADPH kinetics in both experiments (red and black curves in Fig. 4(a)) are due to the tenfold difference in 6PGL quantities, therefore activities ($m_{6PGL} = 150$ ng and $m_{6PGL} = 15$ ng). Assuming that the lactonase activity is the limiting step of the cascade, its activity in the solution with $m_{6PGL} = 150$ ng (black curve in Fig. 4(a)) can be grossly estimated to be $A_{150} \approx 0.04$ U, from a linear interpolation between the first and second plateaus (1U corresponds to the transformation of 1 μmol of substrate per minute). Alternatively, for $m_{6PGL} = 15$ ng (red curve in Fig. 4(a)), the slope of the *linear region of the absorption curve* following the addition of 6PGL, between *c.a.* 3-4 min, leads to $A_{15} \approx 0.005$ U (μmol/min). Therefore, the production rate of NADPH scales with the 6PGL activity (and concentration), and in both cases, the 6PGL activity was clearly far lower than that of 6PGDH. Therefore, in these test experiments, 6PGL was the kinetic limiting step and NADPH, through UV absorption curves (from the first to the second equivalent), represents a spy molecule to monitor 6PGL kinetics. Now, the above conditions were fulfilled in all the inhibition experiments described in this work, as they have been performed with a 6PGDH activity of 0.3 U and with $m_{6PGL} = 15$ ng.

6PGDH activity Measurements of 6PGDH activity were performed by monitoring UV absorption produced from the natural substrate 6PGA (99% purity, Sigma-Aldrich). A 500 μL reaction medium containing [$NADP^+$] = 250 μM, [6PGA] = 100 μM, [Hepes] = 10 mM at pH= 7.5 and $U_{6\text{PGDH}} = 88.10^{-3}$ U was prepared from the stock solutions described above. Various amounts of the inhibitor were added from stock solutions to prepare reactive media with 0, 100, 200, 340 and 800 μM of GP269.

IC_{50} determination The determination of the IC_{50}, i.e., the concentration of inhibitor necessary to halve the reaction rate of the enzymatic reaction, was based on the fitting of the linear region of the UV absorption kinetics curves. The extracted slopes $\Delta(c)$ obtained for different inhibitor concentrations c were first corrected for spontaneous hydrolysis Δ_{sh}. The obtained values $a(c) = \Delta(c) - \Delta_{sh}$ were then fitted to the logistic function:

$$a(c) = \frac{a_0}{1 + (c/\text{IC}_{50})^{1/d_c}}, \tag{3}$$

where a_0 is the activity corresponding to vanishing inhibitor concentration. Results of duplicate experiments were merged together to perform a global fit of the slopes extracted from all performed experiments. The normalized activity $A_n(c)$ was computed as $A_n(c) = \frac{a(c)}{a_0}$.

In silico studies

Docking

For the docking of GP269, the *Tb*6PGL target structure was prepared from the x-ray protein structure of the crystallized complex *Tb*6PGL:6PGA (Protein Data Bank code: 3E7F). Polar hydrogen atoms were added to the protein. The side chains of residues R200, R77 were protonated while H165 was doubly protonated, and residues D75 and D163 were in their aspartate form. The docking of GP269 into the structure of *Tb*6PGL was performed using the SwissDock server [18] which is a web implementation of the EADock DSS algorithm.[19] The latter uses a scoring function designed around the CHARMM22 all-atom force field[20] and the FACTS implicit solvent model[21] to predict the ligand binding modes. Simulation grid had dimensions $30 \times 30 \times 32$ Å and was centered on the position of atom C4 of the 6PGA ligand found in the experimental x-ray structure.[22] Side-chains found within a 5Å radius from the ligand were made flexible during the docking process.

All-atom molecular dynamics

The best scoring binding modes of the protein:ligand complex obtained by the docking protocol were then refined by subsequent energy minimization and all-atom molecular dynamics simulations in explicit solvent. MD simulations were performed with the GROMACS software.[23] We used the AMBER ff99SB-ildn force field [24] and the Generic Amber Force Field (GAFF) to model all the interactions involving both protein and ligand atoms.
The system to be simulated was built by adding around 9000 water molecules in a periodic cubic box of side 68 Å. Water molecules were modelled by 4-particle TIP4P-Ew force field.[25]

The resulting structure was minimized in order to remove possible steric clashes. System equilibration was performed in two steps. Firstly, in order to allow for correct relaxation of the water molecule around the protein, the system was equilibrated over 50000 steps (100 ps) in a NVT ensemble using positional restraints to all the protein atoms. Temperature control was achieved by a modified Berendsen thermostat with a 0.1 ps relaxation time.[26] A further equilibration was performed for additional 1 ns at 1 atm constant pressure by a Parrinello-Rahman barostat with relaxation time of 2 ps.[27] We used a 10.4 Å cutoff radius for range-limited interactions, with Particle Mesh Ewald electrostatics evaluated every fifth step using a fifth-order spline interpolation on an FFT grid with maximum spacing equal to 0.16

nm. A time step of 1 fs was used in the simulations, with long-range electrostatics evaluated every other time step. The configuration with a volume that was the closest to the average volume in this short simulation was extracted and used as input for the production runs in a NVT ensemble. Random velocities reassignment was used to perform three independent production runs of 5 ns for a total 15 ns for each simulated system. To help the analysis of the structural effects of ligand binding, the unbound 6PGL was also modeled starting from the x-ray structure with PDB code 2J0E and MD simulations of the corresponding solvated system were performed following the aforementioned protocol.

For the determination of the bonding network in the active site, distances between centroids of oppositely charged groups were computed, using the following definitions. The centroid positions were calculated as the average position of the heavy atoms involved. Thus, the Arg centroid C^{ARG} was defined by C_ζ, N_ϵ, $N_{\eta 1}$ and $N_{\eta 2}$. Alternatively, C^{HIS} was calculated from the C_γ, $C_{\delta 1}$, $N_{\delta 2}$, $C_{\epsilon 1}$ and $N_{\epsilon 2}$ atoms. Finally, N_ϵ and P were used for C^{LYS} and C^{GP269}.

Results and Discussion

Chemical synthesis of a 6PGL lactam analog of the substrate

The design of the inhibitor was based on simple considerations about the enzyme substrate, the 6-phosphogluconolactone, and was in fact conceived as an analogue of the substrate. Therefore, a lactam analogue of the δ-6-phosphogluconolactone was synthesized from commercially available D-Glucose. The various stages of the synthesis protocol is schematically represented in Fig. 1. Thus, the thioglycoside **2** bearing a silyl ether protected group in 6-position was obtained in 5 steps from D-glucose according to literature procedures.[28] The thiol ether group was then hydrolyzed giving hemiacetal **3** which was efficiently oxidized in smooth oxidation condition with Ac_2O in DMSO, with 81% yield. The amide **5**, prepared from lactone **4** by treatment with ammonia in MeOH (96% yield), was oxidized again with Ac_2O/DMSO giving ketone amide **6**. This unstable intermediate was directly converted into lactame **7** in 44% yield over two steps, through a reductive dehydroxylation reaction. Selective removal of the silyl ether gave the alcohol, which was phosphorylated in 2 steps conducting to phosphorylated lactame **9** in 65% yield. Final hydrogenolysis of all the benzyl groups allowed to reach the desired compound **10** in 73% yield. The end product, GP269, shows no evidence of spontaneous hydrolysis or isomerisation and was thoroughly characterized by ^{1}H and ^{13}C NMR spectroscopy (see Supplementary Information).

NMR spectrocopy

In a first round of experiments aiming at the characterization of the ligand/6PGL interactions, simple NMR experiments were performed to assess the binding of GP269 with 6PGL. Thus, a series of 2D ^{15}N-^{1}H HSQC experiments was performed with increasing amounts of the ligand, with the following ligand to enzyme ratios: 0.33, 1, 2, 5 and 10 (Fig. 2(a)). From these experiments, a number of previously assigned peaks [29] was easily identified on the 2D experiment. On average, the difference of chemical shift perturbations on the 2D ^{15}N-^{1}H HSQC of 6PGL with respect to the values previously published was $\approx 0.03 \pm 0.01$ ppm. Peaks with ambiguous assignments were discarded. In the situation of fast exchange, the slight and progressive shifts of the resonances observed in the successive spectra upon titration were monitored. A quantification of the combined (^{15}N, ^{1}H) chemical shift alterations upon ligand binding was performed using the chemical shift perturbations (CSP) $\Delta\delta$, defined as $\Delta\delta = |\Delta\delta_H| + |\Delta\delta_N/7|$ ($\Delta\delta = |\Delta\delta_H| + |\Delta\delta_N/5|$ for Glycines),[15] where $\Delta\delta_N$ and $\Delta\delta_H$ are the amide ^{15}N and ^{1}H chemical shift displacements of the protein in the presence and the absence of the ligand. In order to extract a value of K_d, we considered the 25 residues displaying CSP values larger than $\langle CSP \rangle + \sigma_{\text{CSP}} = 0.10$ ppm for ligand:enzyme concentration ratio of 10:1 (see Fig. 2(b)). The CSP variations of these residues upon titration were fitted to Eq. 1. The extracted values ranged between 1.0 μM and 17.3 μM (RMSD 4.05 μM). The value of K_d averaged over all the residues was $\langle K_d \rangle = 8.7 \pm 2.4$ μM. Moreover, the value of the dissociation constant obtained by fitting the average CSP over all the residues listed above, for each ligand concentration, was very similar, $K_d = 8.6 \pm 1.3$ μM (see Fig. 2(c)).

An additional set of resonances disappeared upon addition of 0.33 equivalent of GP269, the smallest amount used in our experiments, and no CSP value could be computed for the corresponding amino acids. This provided evidence of an intermediate exchange regime, and the presence of protein motions between several conformations on slow time scales. Interestingly, a number of residues with high CSP variations, i.e., larger than $\langle CSP \rangle + 2\sigma_{\text{CSP}} = 0.16$ ppm at a ligand:enzyme ratio of 10, are close neighbours of the latter. Taken together, these two kinds of amino acids define three 6PGL regions that very sensitive to ligand binding. As illustrated in Fig. 2, this includes A41-G45, L157-F170, and A218-K223 protein segments. Note that the appearance of sparse resonances was observed at 5 and 10 GP269 equivalents but the complete assignment of the bound 6PGL has not been performed at this stage.

GP269 is a 6PGL inhibitor

The enzymatic activity of 6PGL was assessed through the observation of NADPH produced during the enzymatic cascade, using UV spectroscopy. Indeed, NADPH is formed through the actions of the G6PDH and 6PGDH enzymes, both of which use $NADP^+$ as a cofactor (Fig. 3).

Thus, NADPH is first produced during the synthesis of δ-6-phosphogluconolactone through oxidation of Glucose-6-Phosphate by G6PDH, and at the later stage of 6-phosphogluconic acid decarboxilation by 6PGDH that yields ribulose-5-Phosphate (see Figure 3). NADPH concentration was monitored through a characteristic UV absorption peak at 340 nm, which allows to distinguish it from the $NADP^+$ cofactor, with which it shares two additional absorption peaks around ~ 215 nm and ~ 255 nm.
The experiment works as follows. In order to ensure that the lactonase activity of 6PGL was the kinetically limiting step of the cascade, much larger G6PDH and 6PGDH activities were used in the reaction medium. Upon addition of G-6-P (at $t_0 = 1$ min) an initial steep rise of UV absorption ($t < 3$ min) by NADPH produced through the action of G6PDH is observed (see Fig. 4(a)). It is followed by a second increase of UV absorption, indirectly attesting for the production of 6PGA, through its subsequent decarboxilation by 6PGDH and the associated NADPH creation. In the absence of 6PGL, this latter process is very slow, and corresponds to 6PGA production through spontaneous hydrolysis of the lactones (see Fig.3).[30] Alternatively, when large quantities of 6PGL are used (150 ng), the second stage of UV absorption is very fast, and has almost reached its plateau by the time measurements are performed again after sample handling for the introduction of 6PGL (Fig. 4(a)).
In the intermediate case where 6PGL activity is moderate (provided by 15 ng of the protein), the UV kinetics curve is linear in the region 5 min $\leq t \leq$ 8 min. This constant rate of NADPH formation therefore indicates a pseudo zero-order hydrolysis kinetics with respect to δ-phosphogluconolactone. Under these conditions, 6PGL activity was thus extracted from the linear part of the kinetic curve.

Interference of both reactions was avoided by initiating 6PGL hydrolysis after G6PDH action was complete. The time of completion of the first reaction (G6PDH), τ_0, was estimated by fitting the initial part of the curve to an empirical bi-exponential function (Eq.2). The faster time constant, corresponding to the initial rise of the UV curve was $\tau_1 \approx 20$ s in the absence of 6PGL. Therefore the delay $\tau_0 - t_0 = 2$ min ($\approx 6 \times \tau_1$) following the addition of G-6-P was used (τ_0 was fixed to 3 min, the starting time of the G6PDH kinetics experiments being $t_0 = 1$ min).
Inhibition of 6PGL by GP269 is clearly demonstrated in Figure 4(b), where the slopes of the kinetics curves systematically decay for increasing concentrations of the ligand (1 μM, 2.5 μM, 5 μM, 10 μM, 25 μM, 50 μM, 100 μM, and 250 μM). In order to provide quantitative values of 6PGL activity upon inhibition, to further characterize inhibition by extracting an IC50 from our data, the contribution of spontaneous hydrolysis was assessed by estimating the longer time constant τ_2 in Eq. 2. Owing to the large extracted value $\tau_2 \approx 34$ min on the observation time scale, a linear approximation of the kinetics was justified and an estimate of this spontaneous hydrolysis "activity" was simply given by the slope Δ_{sh} of the UV absorption curve. Thus, using this approximation, 6PGL activities under various inhibitor

concentrations were obtained as the differences between the observed kinetics and Δ_{sh} (see *Materials and Methods*).

For each ligand concentration [GP269], a quantitative analysis was performed by fitting the initial linear regions of the absorption curves to straight lines. Thus, the kinetics in this time interval occurs with constant reaction rates, and therefore correspond to pseudo zero-order kinetics in δ-6-phosphogluconolactone, in large excess at the early stage of the enzymatic hydrolysis by *Tb*6PGL (see *Materials and Methods* for details). Results are shown in Fig. 5, and the numerical values of the slopes are given in Table 1

Surprisingly, additional 6PGDH inhibition by GP269 was suspected from the observation that the spontaneous hydrolysis of the lactone was faster than the 6PGL-catalyzed hydrolysis at large inhibitor concentrations ($[GP269] = 250\ \mu$M). This was confirmed by inhibition experiments using 6PGA as the substrate, and inhibitor concentrations in the range [0;800] μM. Thus, 6PGDH is inhibited by GP269, albeit at concentrations higher than 100 μM (see Table 2 and Fig. 1 in the *Supplementary Information*). The values of the 6PGL activities were therefore analyzed in the presence of increasing concentrations of GP269, up to 100 μM, in order to extract an IC_{50} value for the inhibitor and to avoid simultaneous inhibitory effects on both enzymes. Using Eq. 3 and data from both series of experiments, we obtained an $IC_{50} = 11.1 \pm 1.6\ \mu$M (Fig. 6).

Docking and MD simulations

In an effort to further characterize the interactions between the protein and its inhibitor, we performed Docking and MD simulation studies. The docking protocol, including the force field and strategy are described in *Materials and Methods*. Thus, docking studies yielded 256 possible conformations of GP269 in the 6PGL active site. These were ranked according to the scoring functions defined within the framework of the algorithm EAdock DSS.[19, 18, 31] According to the latter, the docked ligands are first ranked by the so-called *SimpleFitness* scoring function which is the sum of the intra- and inter- molecular energy terms of the protein:ligand complex calculated using the CHARM22[20] force field. The resulting conformations are then clustered with respect to their RMSDs and clusters are ranked by the *FullFitness* protocol that adds a solvation free energy term, evaluated by the FACTS implicit model[21], to the previous scoring function.

Interestingly, among the best scoring poses of GP269, two clusters of conformations emerged. In one of them, the ligand appears to be docked into the active site of the enzyme, with its lactam ring in the vicinity of the Arg77 and Arg200 residues. In this case, the phosphate group points outwards, but remains relatively close (4.7 Å) to the N^{ζ} nitrogen atom of the Lys223 side chain, and to the $N^{\epsilon 2}$ of His165 (5.0 Å), too. Alternatively, in the second cluster,

the ligand is slightly tilted with respect to the previous case. Here, the phosphate group is located halfway between the N^{η} nitrogen atoms of Arg77 and Arg200 side chains ($\sim$ 4.0 Å) on one side, and the $N^{\epsilon 2}$ atom of His165 (3.7 Å) on the other. Consequently, due to this orientation, the lactam group reaches a region that is in the vicinity of residues G44 and G45. For each cluster a representative pose was selected according to its score. As expected, the first cluster yields conformation (CONF1), associated with the best *FullFitness* scoring. More surprisingly, the second cluster contains the binding pose (CONF2), which has the best *SimpleFitness* score. These two conformations were chosen as exemplars of the two clusters and were retained for further analysis. Both are represented in Figure 7, and ranking and scoring results of the selected conformations are indicated in Table (2). Interestingly, both CONF1 and CONF2 poses share very similar *SimpleFitness* scoring, whereas their *FullFitness* values are slightly different ($\sim$ 5 kcal/mol). Nevertheless, this difference is by far smaller than the expected error ($\sim$ 3%) associated with the evaluation of solvation energies by the FACTS algorithm.[21] Therefore, the two GP269:6PGL poses should be considered practically equivalent from the energy point of view.

The GP269 docking poses found during this study are consistent with those found for the lactone counterpart and discussed in Ref [11]. In particular, the CONF1 pose (Fig. 7(a)), in which the phosphate group points towards the Lys223 residue, is also consistent with the substrate binding pose in the NagB family. In the lactone case, this pose suggested an activation mechanism involving the protonated $N^{\epsilon 2}$ atom of His165 in close contact with the oxygen atom of the pyranose ring of the substrate.

Alternatively, the CONF2 case (Fig. 7(b)) is compatible with the second cluster of orientations proposed in [11], for which a possible activation of the ring opening was mediated by the guanidinium group of Arg77 close to the oxygen in the lactone ring. Conversely, in the case of GP269 in CONF2, the ring nitrogen is found halfway between His165 and Arg77. Moreover, it is worth noting that the phosphate group is located at a position that is only 0.3 Å away from its 6PGA counterpart, as observed in the crystal structure of the 6PGL:6PGA complex (PDB code: 3E7F).[22]

Ligand-protein interactions In order to specify the various intermolecular interactions between GP269 and 6PGL that docking suggested, three independent 5 ns MD simulations were performed on both 6PGL:GP269 complex conformations. Convergence was reached, as attested by the C_{α} RMSD (see *Supplementary Information*). These short MD simulations were used to assess the kinetic stability of each complex[32, 33] rather than to explore the protein internal motions.[34] They also served to clarify the weak bonding network that stabilizes the complex, such as ion-pair interactions and hydrogen bonds, through the analysis of atomic distances between 6PGL and GP269.

Distances between the phosphate group and different amino acids in the 6PGL active site for CONF1 and CONF2 are shown in Figures 8 and 9. The presence of salt bridges was inferred from the MD simulations when the following conditions were simultaneously fulfilled: [35] *i)* the distance between the centroids of oppositely charged groups are $\leq$ 4.0 Å, and *ii)* there exists at least one pair of {phosphate oxygen, nitrogen} atoms distant by $\leq$ 4.0 Å. If either of these conditions is violated,[36, 37] two other kinds of ion-pair interactions may exist. These are the "N-O bridges", when only *i)* is not verified, and "long-range" electrostatic interaction if inter-atom distances fail to fulfill both conditions. The strengths of these electrostatic interactions decrease from salt bridges to longer-range ion pairs.
In CONF1, the phosphate group of GP269 is located in the region between His165 and Lys223. Our analysis shows that its distance with the side chain of Lys223 is suggestive of a salt bridge, whereas the side chain of His165 is essentially localized within a distance that is consistent with a N-O bridge interaction. Interestingly, in CONF2 the phosphate group is involved in a somewhat larger number of electrostatic interactions. Indeed, it is located at a distance from His165 that is compatible with an N-O bridge, and in addition seems to form longer-range ion pairs with both Arg77 and Arg200 in the active site. These results are summarized in Figs. 8 and 9. The fact that only one significant salt-bridge interaction was detectable in CONF1, whereas the ligand is involved in a network of weak ion-pair interactions involving His165, Arg77 and Arg200 in CONF2 is consistent with previous results on the 6PGL:6-phosphogluconolactone complex,[22] and suggests that GP269 may interact with the active site similarly to the enzyme's own substrate.

In order to investigate the existence of further analogies between the inhibitor and the substrate, the existence of specific hydrogen bond networks was also investigated. To this aim, the usual angle-distance criteria were applied, according to which a hydrogen bond is assumed when the donor-acceptor distance is $<$ 3.0 Å and the angle donor-H-acceptor is less than 20 degrees. Thus, donor-acceptor pairs that persisted for more than 20% of the overall MD length (15 ns) were identified. Results are listed in Table 3.

In both conformations, possible interactions were detected between the ligand and residues Gly44 and Asp75 in the active site. Surprisingly, only two donor-acceptor pairs seemed to exist in CONF2, both with an occupancy smaller than 50%, indicating a rather unlikely hydrogen bond formation. However, separate analyses of the MD simulation runs showed that in two out of three runs, both donor-acceptor pairs are likely to form hydrogen bonds. In contrast, these interactions completely disappear from the third simulation (see Table 4). This difference is due to a conformational change in GP269 during the last simulation run, where the lactam ring moves from a region in close vicinity of Gly44 and Gly45 towards Lys223. This is clearly shown in Figure 10 (lower panel). Interestingly, in this alternate conformation, the O6 and O7 oxygen atoms of the lactam ring remain within a distance of 3 Å from the amino group of Lys223 during most of the simulation time (see Figure 10), although without satisfying

the hydrogen bond criteria. Moreover, this tilt of GP269 occurs without significant changes of the phosphate group position, which remains close to Arg77 and Arg200. Note that the independence of the three simulation runs ensures that the observed differences in CONF2 are sampled from the statistical fluctuations of the 6PGL:GP269 complex, although it is of course not possible to determine their respective weights from just these MD simulations. Besides, since for this pose the overall orientation of GP269 is similar to the previously determined X-ray conformation of the natural reaction product 6PGA,[22] this somehow suggests that such a conformational change of the complex might be involved as a precursor state of ligand unbinding.

Comparison with NMR experiments Finally, the proximities between ligand and enzyme atoms evidenced by the docking calculations, as well as the H-bond network and ion-pair interactions identified by MD simulations, are complementary to the experimental NMR titration of 6PGL by GP269. In the latter case, a number of residues undergo intermediate exchange upon titration. This indicates the presence of protein slow motions, meaning that a new conformational state is induced by the interaction with GP269. The distribution of these residues is shown in Fig. 11 on the 3D structure of the protein. The NMR experiments performed in this work only provide a chemical exchange signature of ligand binding to 6PGL. Therefore, no straightforward mapping exists between the chemical shift perturbations of nuclei located at a distance from the active site and the protein:ligand inter-atomic weak bonds observed in our MD simulations. Nevertheless, it is clear that the results obtained by MD simulations show consistency with the NMR observations. In particular, several active site residues that are engaged in ion-pair interactions or H-bonds, in either pose, also exhibit conformational exchange in NMR experiments (Lys223, His165, Gly45). Moreover, the CSP values of residues Arg200 and Arg77 were respectively 0.09 and 0.07 ppm. Thus, despite the fact that these were only slightly below the rather stringent significance threshold imposed in the present analysis (0.1 ppm), such values are significant.

A particularly interesting feature is shown in Fig. 11, where the residues that undergo conformational exchange are mapped onto the 3D structure of the docking complex. This clearly shows that these are located in a region of the protein that caps the active site and the ligand binding site, whereas the rest of the protein seems to be largely unaffected by these changes. This gives further credit to the well-established involvement of such protein dynamics in protein-ligand interactions. In any event, it is clear that the dynamics taking place at fast ($\sim$ns) or slow (μs or longer) time scales deserves a study in its own right, both *in silico* and experimental, to provide quantitative results. This is beyond the scope of this article and is delayed to further work.

Conclusion

In this work, a newly synthesized enzymatic inhibitor of the PPP was introduced, designed as a lactam analogue of the 6PGL substrate. This first known inihibitor of 6PGL was characterized in terms of affinity to its primary target, and also of inhibiting power, based on kinetics experiments. This opens new avenues for the future development of strategies against *T. brucei* that target the PPP. These results strongly motivate further studies to thoroughly determine its mechanism of action, including its likely competitive character. Considering its chemical structure, which makes it likely amenable to various chemical modifications, GP269 represents a potential lead for further drug development. Importantly, the results presented here lay the base for future investigations, which should develop along several lines. These include the testing of the actual toxicity of GP269 on various forms of the parasite *T. brucei*. On a more fundamental level, the relation between the docking results and the mobility of the ligand in the active site should be investigated by further *in silico* explorations, as well as NMR dynamical studies of the protein side chains.

Author contributions statement

ATT performed chemical synthesis. AS performed UV experiments. PC carried out in silico studies. PL and JO performed protein expression and purification. MS supervised chemical syntheses and contributed to the writing of the paper. EM conceived the study, performed UV and NMR experiments, and contributed to the writing of the paper. DA coordinated the study and wrote the paper.

Supplemental information

NMR and HRMS characterizations of compounds **3-10**; experimental procedures for UV kinetics measurements and UV data analysis; NMR conditions for titration experiments; RMSD trajectories of the MD simulations.

Acknowledgements

Marie Grimaldi and Paul Robin are gratefully acknowledged for their help with preliminary experiments. The authors declare that they have no conflicts of interest with the contents of this article.

References

[1] M. P. Barrett, R. J. S. Burchmore, and A. Stich et al. The trypanosomiases. The Lancet, 362:1469–1480, 2003.

[2] S. H. Funayama, S. Funayama, I. Y. Ito, and L. A. Veiga. Trypanosoma cruzi:kinetic properties of glucose-6-phosphate dehydrogenase. Experimental Parasitology, 43:376–381, 1977.

[3] P. Büscher, G. Cecchi, V. Jamonneau, and G. Priotto. Human african trypanosomiasis. The Lancet, 390:2397–2409, 2017.

[4] Frederic Opperdoes. Compartmentation of carbohydrate metabolism in trypanosomes. Annual Review of Microbiology, 41:127–151, 1987.

[5] J. Kovárova and M. P. Barrett. The pentose phosphate pathway in parasitic trypanosomatids. Trends in Parasitology, 32:622–634, 2016.

[6] M. P. Barrett, G.H. Coombs, and J.C. Mottram. Recent advances in identifying and validating drug targets in trypanosomes and leishmanias. Trends Microbiol., 1999.

[7] G.J. Crowther, D. Shanmugam, S.J. Carmona, M.A. Doyle, C. Hertz-Fowler, M. Berriman, S. Nwaka, S.A. Ralph, D.S. Roos, W.C. Van Voorhis, and F. Aguero. Identification of attractive drug targets in neglected-disease pathogens using an in silico approach. PLoS Neglected Tropical Diseases, 4:article e804, 2010.

[8] C. L. M. J. Verlinde, V. Hannaert, C. Blonski, M. Willson, J.J. Périé, L.A. Fothergill-Gilmore, F.R. Opperdoes, M.H. Gelb, W.G. Hol, and P.A. Michels. Glycolysis as a target for the design of new anti-trypanosome drugs. Drug Resistance Updates, 4:5–65, 2001.

[9] M. P. Barrett. The pentose phosphate pathway and parasitic protozoa. Parasitology Today, 13:11–16, 1997.

[10] F.R. Opperdoes and P.A. Michels. Enzymes of carbohydrate metabolism as potential drug targets. Int. J. Parasitol., 31:482–490, 2001.

[11] Marc Delarue, Nathalie Duclert-Savatier, Emeric Miclet, Ahmed Haouz, David Giganti, Jamal Ouazzani, Philippe Lopes, Michael Nilges, and Véronique Stoven. Three dimensional structure and implications for the catalytic mechanism of 6-phosphogluconolactonase from trypanosoma brucei. Journal of Molecular Biology, 366:868–881, 2007.

[12] C. Phillips, J. Dohnalek, S. Gover, M.P. Barrett, and M.J. Adams. A 2.8åresolution structure of 6-phosphogluconate dehydrogenase from the protozoan parasite trypanosoma brucei: comparison with the sheep enzyme accounts for differences in activity with coenzyme and substrate analogues. Journal of Molecular Biology, 282:667–681, 1998.

[13] S. Hanau, E. Rinaldi, F. Dallocchio, I.H. Gilbert, D. Dardonville, M. J. M.J. Adams, S. Gover, and M.P. Barrett. 6-phosphogluconate dehydrogenase: a target for drugs in african trypanosomes. Curr. Med. Chem, 11:2639–2650, 2004.

[14] S. Mori, C. Abeygunawardana, M.O. Johnson, and P.C. van Zijl. J. Magn. Reson. B, 108:94–98, 1995.

[15] Mike P. Williamson. Using chemical shift perturbation to characterise ligand binding. Progress in Nuclear Magnetic Resonance Spectroscopy, 73:1–16, 2013.

[16] Francis Duffieux, Joris Van Roy, Paul A. M. Michels, and Fred R. Opperdoes. Molecular characterization of the first two enzymes of the pentose-phosphate pathway of trypanosoma brucei. J. Biol. Chem., 275:27559–27565, 2000.

[17] Scilab, a free scientific software package. Copyright 1989-2005. INRIA ENPC,www.scilab.org.

[18] Aurélien Grosdidier, Vincent Zoete, and Olivier Michielin. Swissdock, a protein-small molecule docking web service based on eadock dss. Nucleic Acids Res, 39:W270–7, 2011.

[19] Aurélien Grosdidier, Vincent Zoete, and Olivier Michielin. Fast docking using the charmm force field with eadock dss. J Comput Chem, 32:2149–59, 2011.

[20] A D MacKerell, D Bashford, M Bellott, R L Dunbrack, J D Evanseck, M J Field, S Fischer, J Gao, H Guo, S Ha, D Joseph-McCarthy, L Kuchnir, K Kuczera, F T K Lau, C Mattos, S Michnick, T Ngo, D T Nguyen, B Prodhom, W E Reiher, III, B Roux, M Schlenkrich, J C Smith, R Stote, J Straub, M Watanabe, J Wiórkiewicz-Kuczera, D Yin, and M Karplus. All-atom empirical potential for molecular modeling and dynamics studies of proteins. Journal of Physical Chemistry B, 102:3586–3616, 1998.

[21] Urs Haberthür and Amedeo Caflisch. Facts: Fast analytical continuum treatment of solvation. J Comput Chem, 29:701–15, 2008.

[22] Nathalie Duclert-Savatier, Luisa Poggi, Emeric Miclet, Philippe Lopes, Jamal Ouazzani, Nathalie Chevalier, Michael Nilges, Marc Delarue, and Véronique Stoven. Insights into

the enzymatic mechanism of 6-phosphogluconolactonase from trypanosoma brucei using structuraldata and moleculardynamics simulation. Journal of Molecular Biology, 388:1009–1021, 2009.

[23] B Hess, C Kutzner, D Van Der Spoel, and E Lindahl. Gromacs 4: Algorithms for highly efficient, load-balanced, and scalable molecular simulation. Journal of chemical theory and computation, 4(3):435–447, 2008.

[24] Kresten Lindorff-Larsen, Stefano Piana, Kim Palmo, Paul Maragakis, John L Klepeis, Ron O Dror, and David E Shaw. Improved side-chain torsion potentials for the amber ff99sb protein force field. Proteins, 78(8):1950–8, Jun 2010.

[25] Hans W Horn, William C Swope, Jed W Pitera, Jeffry D Madura, Thomas J Dick, Greg L Hura, and Teresa Head-Gordon. Development of an improved four-site water model for biomolecular simulations: Tip4p-ew. J Chem Phys, 120:9665–78, 2004.

[26] Giovanni Bussi, Davide Donadio, and Michele Parrinello. Canonical sampling through velocity rescaling. J Chem Phys, 126:014101, 2007.

[27] M Parrinello and A Rahman. Polymorphic transitions in single crystals: A new molecular dynamics method. J. Appl. Phys., 52:7182–7190, 1981.

[28] Edward I. Balmond, Diane M. Coe, M. Carmen Galan, and Eoghan Mcgarrigle. α-selective organocatalytic synthesis of 2-deoxygalactosides. Angew. Chem. Int. Ed, 2012.

[29] E. Miclet, F. Duffieux, J.-Y. Lallemand, and V. Stoven. Backbone hn,n,cα,ca, and cβ assignment of the 6-phosphogluconolactonase, a 266-residue enzyme of the pentose-phosphate pathway from human parasite trypanosoma brucei. J. Biomol. NMR, 25:249–250, 2003.

[30] E. Miclet, V. Stoven, Paul A. M. Michels, Frederic R. Opperdoes, J.-Y. Lallemand, and F. Duffieux. Nmr spectroscopic analysis of the first two steps of the pentose-phosphate pathway elucidates the role of 6-phosphogluconolactonase. J. Biol. Chem., 276:34840–34846, 2001.

[31] Vincent Zoete, Michel A Cuendet, Aurélien Grosdidier, and Olivier Michielin. Swissparam: a fast force field generation tool for small organic molecules. J Comput Chem, 32:2359–68, 2011.

[32] Vincent Zoete, Markus Meuwly, and Martin Karplus. Investigation of glucose binding sites on insulin. PROTEINS: Structure, Function, and Bioinformatics, 55:568–581, 2004.

[33] Hwangseo Park, Min Sun Yeom, and Sangyoub Lee. Loop flexibility and solvent dynamics as determinants for the selective inhibition of cyclin-dependent kinase 4: Comparative molecular dynamics simulation studies of cdk2 and cdk4. ChemBioChem, 5:1662–1672, 2004.

[34] Paolo Calligari, Gilmar Salgado, Philippe Pelupessy, Jamal Ouazzani, Philippe Lopes, Geoffrey Bodenhausen, and Daniel Abergel. Insights into internal dynamics of 6-phosphogluconolactonase from trypanosoma brucei studied by nmr and molecular dynamics. Proteins: Structure, Function, and Bioinformatics, 80:1196–1210, 2012.

[35] Sandeep Kumar and Ruth Nussinov. Relationship between Ion Pair Geometries and Electrostatic Strengths in Proteins. Biophys J, 83(3):1595–1612, 2002.

[36] Sandeep Kumar and Ruth Nussinov. Close-Range Electrostatic Interactions in Proteins. ChemBioChem, 3(7):604–617, 2002.

[37] Sandeep Kumar and Ruth Nussinov. Salt bridge stability in monomeric proteins1. J Mol Biol, 293(5):1241–1255, 1999.

Tables

Inhibitor concentration (μM)	250	100	50	25	10	5	2.5	1	0
average slope (1) (μM.min^{-1})	0.58	1.03	1.44	1.79	2.43	2.62	3.13	3.42	3.54
average slope (2) (μM.min^{-1})	0.66	1.23	1.54	1.80	2.65	3.03	3.50	3.52	3.97

Table 1: Slopes $\Delta(c)$ extracted from the NADPH UV absorption curves recorded in the presence of 6PGL at different concentrations of the inhibitor. Two series of experiments have been performed and slopes have been determined in duplicate. The molar extinction of NADPH at $\lambda = 340$ nm is $\epsilon = 6300$ M^{-1}.cm^{-1}. Data points acquired between $t = 5$ min and $t = 8$ min were used for fitting. In the absence of 6PGL, the slope $\Delta_{sh} = 1.04$ μM.min^{-1} was obtained.

	FullFitness	FullRank	SimpleFitness	SimpleRank
CONF1	-1619.87	1	-80.07	5
CONF2	-1614.21	5	-81.89	1

Table 2: Ranking and scoring for the two configurations selected for further analysis. The *FullRank* and *SimpleRank* columns show the ranking of each pose with respect to the *FullFitness* and *SimpleFitness* scoring functions, respectively. All the values are expressed in kcal/mol.

Conformation	donor	acceptor	occupancy (%)
CONF1	ASP75-$O_{\delta 1}$	GP269-O3	70.75%
	GP269-O2	ASP75-$O_{\delta 2}$	61.09%
	ARG200-$N_{\eta 1}$	GP269-O1	59.15%
	GLY44-Main-N	GP269-O3	24.31%
CONF2	GP269-O4	ASP75-$O_{\delta 1}$	49.25%
	GP269-O2	GLY44-O	31.49%

Table 3: Hydrogen bonds between GP269 and 6PGL. Hydrogen bonds are detected along the production runs. Only pairs with occupancy larger than 10% are shown.

Figures

Conformation	donor	acceptor	occupancy (%)		
CONF2	GP269-O4	ASP75-$O_{\delta 1}$	75.90%	68.60%	3.27%
	GP269-O2	GLY44-O	37.36%	54.29%	2.83%

Table 4: Hydrogen bonds between GP269 and 6PGL. Hydrogen bonds are detected along the three production runs.

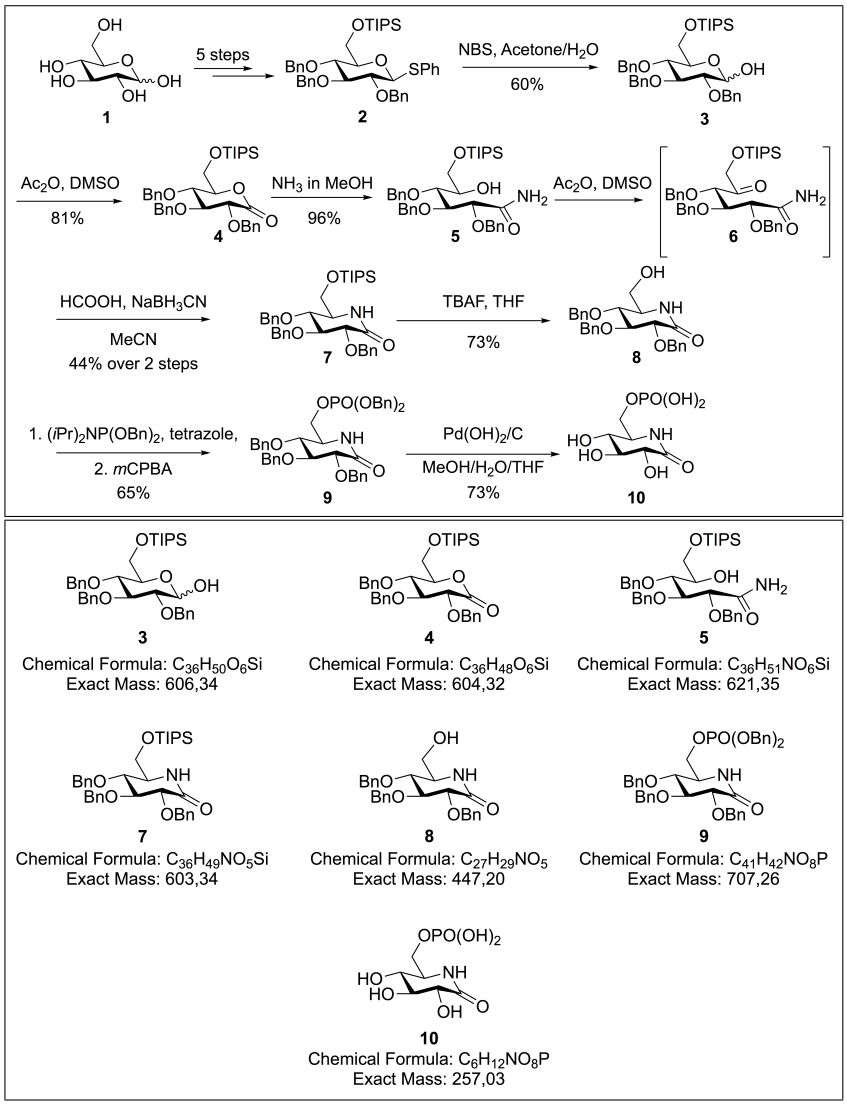

Figure 1: Synthesis overview of GP269 (compound **10**).

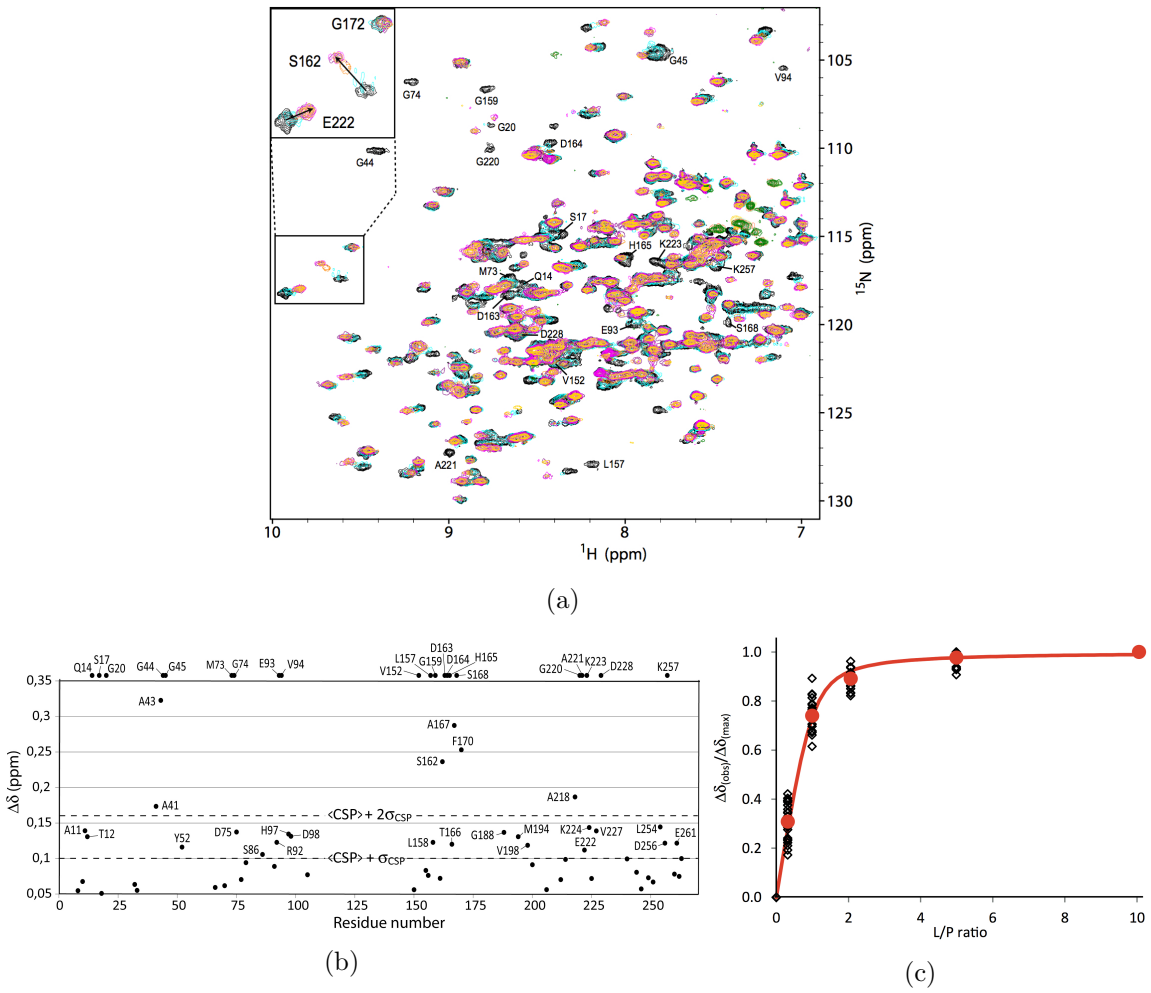

Figure 2: 2(a) Overlay of the [^{1}H-^{15}N]-HSQC spectra of a 90 μM sample of *Tb*6PGL obtained upon GP269 titration. The assigned peaks on the full spectrum correspond to residues that disappear with 0.33 Eq. GP269 (residues in intermediate exchange). In the inset, examples of residues in fast exchange (S162 and E222) are shown together with the G172 peak, which is unaffected by addition of the ligand; 2(b) Residues with significant CSP shifts upon ligand addition (A11, T12, A41, A43, Y52, D75, S86, R92, H97, D98, L158, S162, T166, A167, F170, G188, M194, V198, A218, E222, K224, V227, L254, D256, E261) are shown. Residues exhibiting intermediate exchange, as attested by the disappearance of their NMR peaks, are indicated above the graph. 2(c): CSP measured during titration of the residues in fast exchange and obtained with 0, 0.33, 1, 2, 5 and 10 equivalent of GP269 (open diamonds). Red filled circles indicate the average of CSP over all used residues, for each G-6-P concentration. The red line is the associated fit, with $Kd = 8.6 \pm 1.3$ μM.

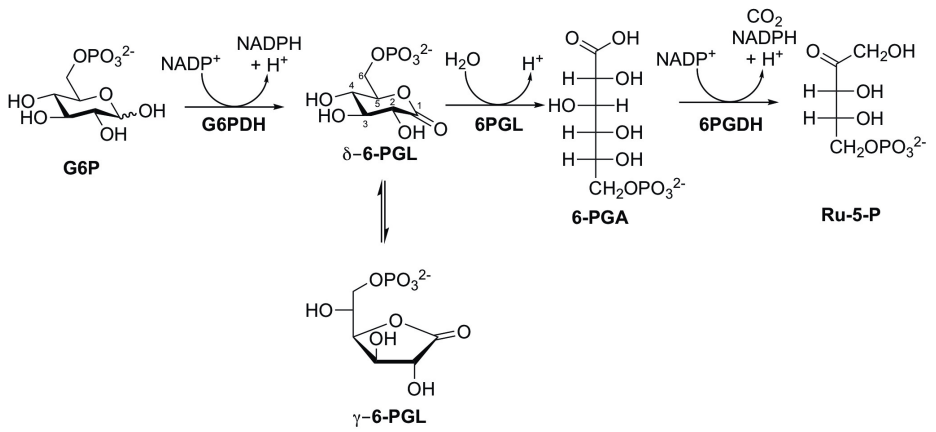

Figure 3: Schematic representation of the oxidative stage of the PPP. In the absence of 6PGL, δ-6-phosphogluconolactone undergoes spontaneous hydrolysis into 6PGA.

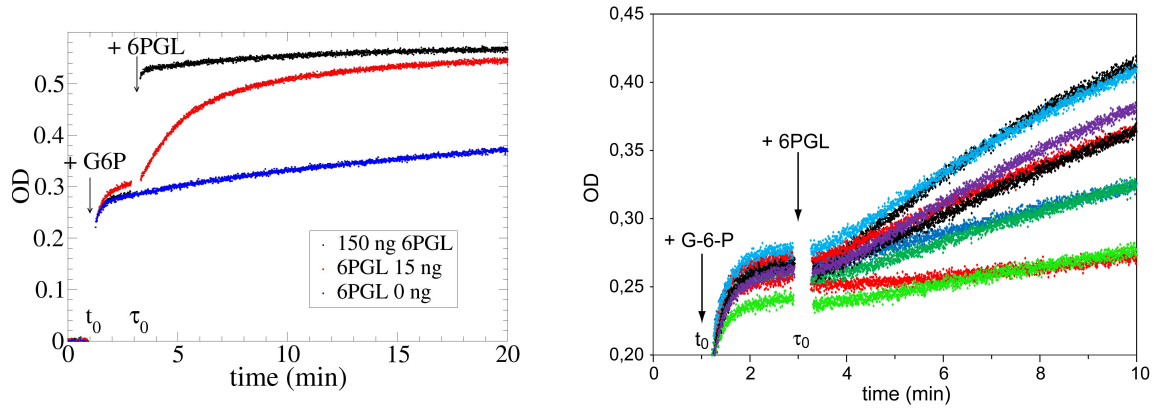

(a) (b)

Figure 4: Monitoring of 6PGL enzymatic activity through UV absorption. a) The first steep rise ($t_0 = 1$ min) corresponds to UV absorption by NADPH produced by G6PDH upon G-6-P addition. The next UV absorption jump at $\tau_0 = 3$ min in the black and red curves corresponds to NADPH creation associated with 6PGA decarboxilation by 6PGDH. Data were obtained for 150 ng (black) and 15 ng (red) 6PGL. In the absence of 6PGL (blue curve), the slow slope corresponds to spontaneous lactone hydrolysis into 6PGA. Experimental conditions are given in Table 1 in the *Supplementary Information*. b) 6PGL kinetics obtained for increasing concentrations of GP269: 0 μM (black), 1 μM (cyan), 2.5 μM (purple), 5 μM (black), 10 μM (red), 25 μM (dark green), 50 μM (blue), 100 μM (light green), 250 μM (red). The linear part of the NADPH kinetic curve at $t \geq 5$ min is associated to zero-order kinetics in δ-6-phosphogluconolactone. The different plateau values before addition of 6PGL reflect experimental errors on G-6-P volumes added to the reactive medium at $t = 0$. This error, though irrelevant for our analysis, was estimated to be on the order of 7%.

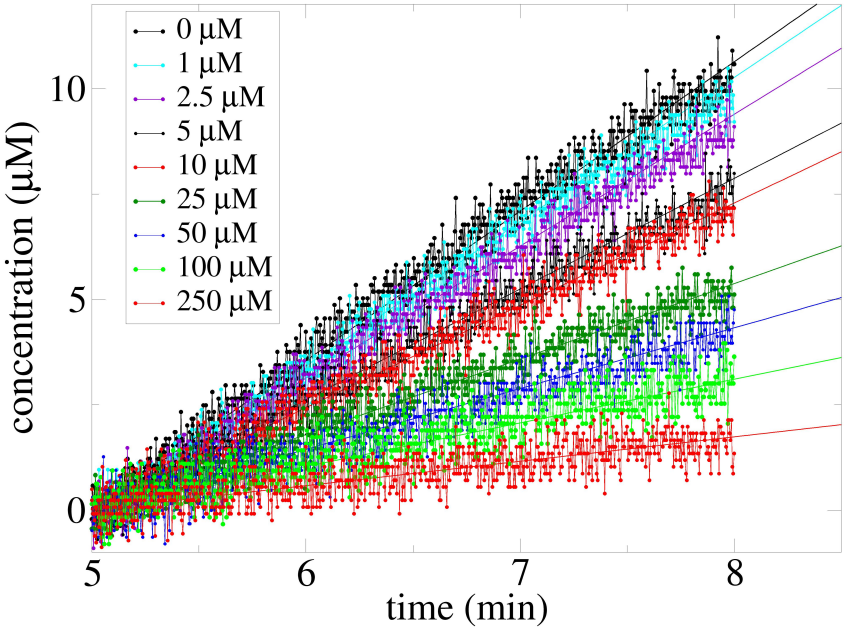

Figure 5: Inhibition experiments - The linear regions of the UV kinetics curves (5 min $\leq t \leq$ 8 min) upon increasing concentrations of GP269, and depicted in Fig. 4, are least-square fitted to straight lines. The relevant GP269 concentrations are indicated in the figure box. The titration has been performed in duplicate, values are given in Table 1.

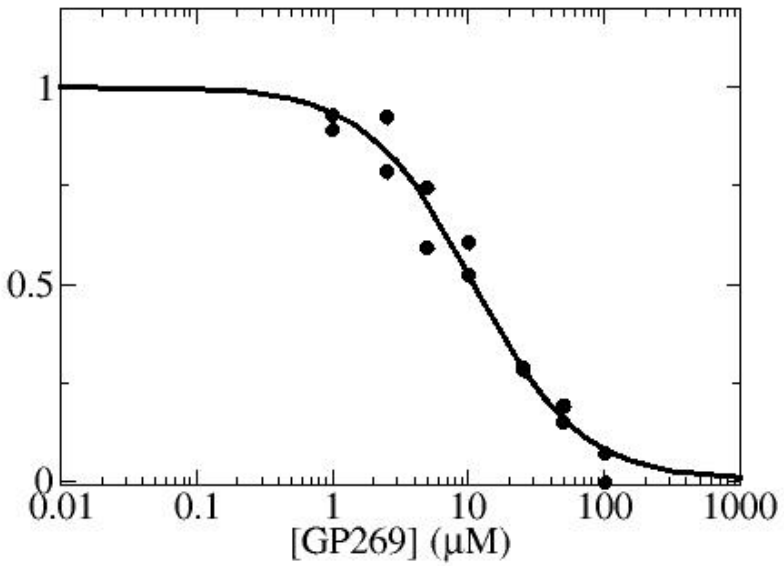

Figure 6: Fit (solid line) of the experimental activities $A_n(c)$ to Eq. 3, for 6PGL. The IC50 concentration corresponds to the inflexion point of the curve.

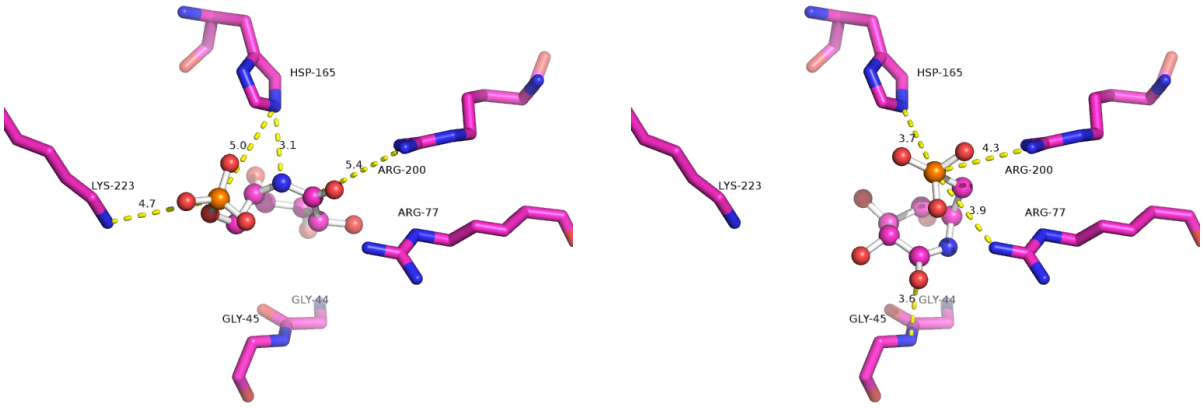

(a) CONF1 (b) CONF2

Figure 7: Docking of GP269 into the 6PGL active site reveals two different poses, depending on the protocol used (see text for details). Only side chains of residues that belong to the active site are shown.

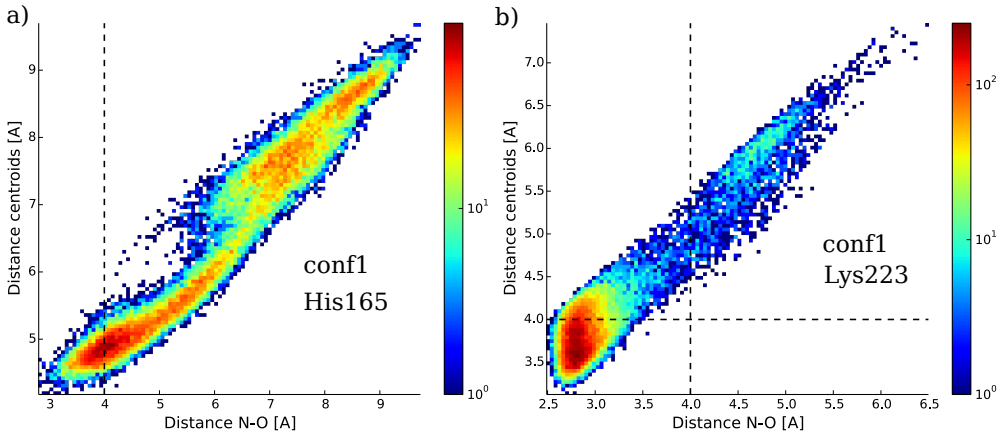

Figure 8: Distances between the GP269 phosphate group and active site residues in CONF1. Dashed lines indicate the boundaries of different ion-pair interaction.

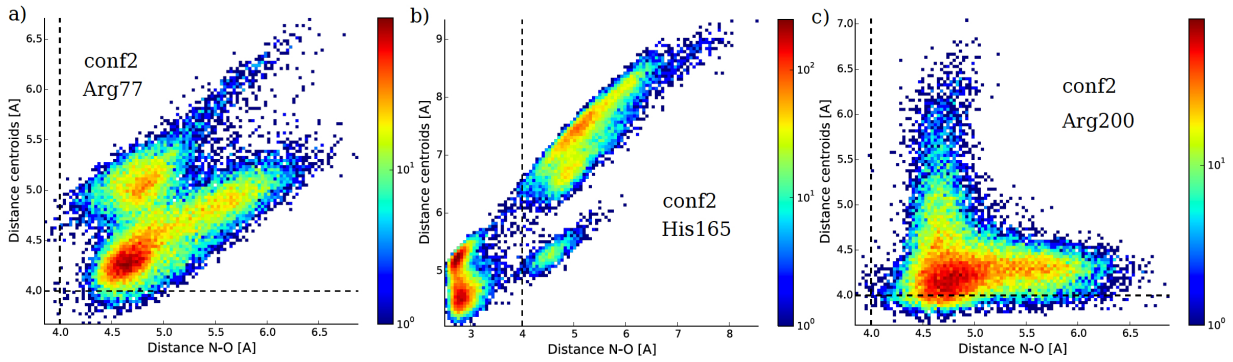

Figure 9: Distances between the GP269 phosphate group and active site residues in CONF2.

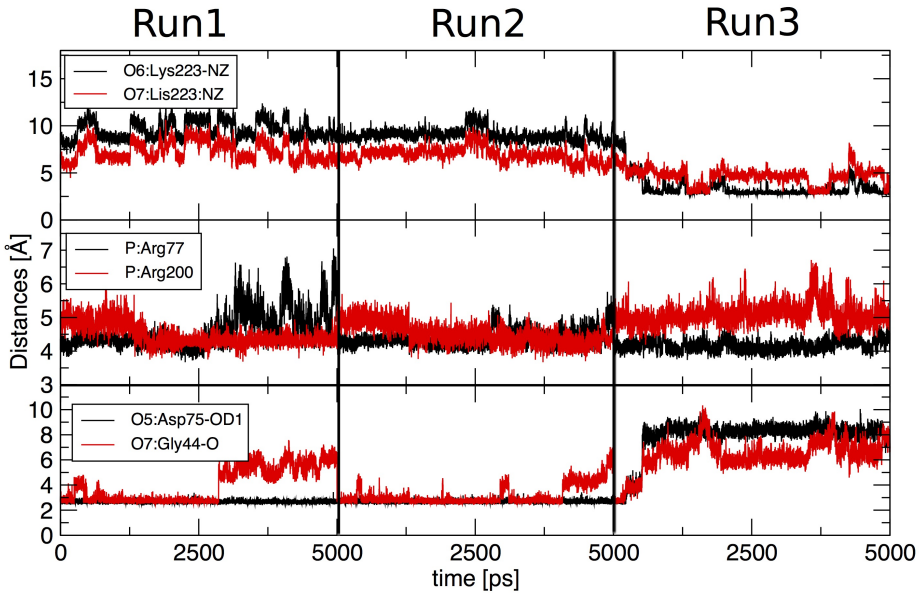

Figure 10: Time evolution of distances between GP269 in CONF2 conformation and residues in the active site.

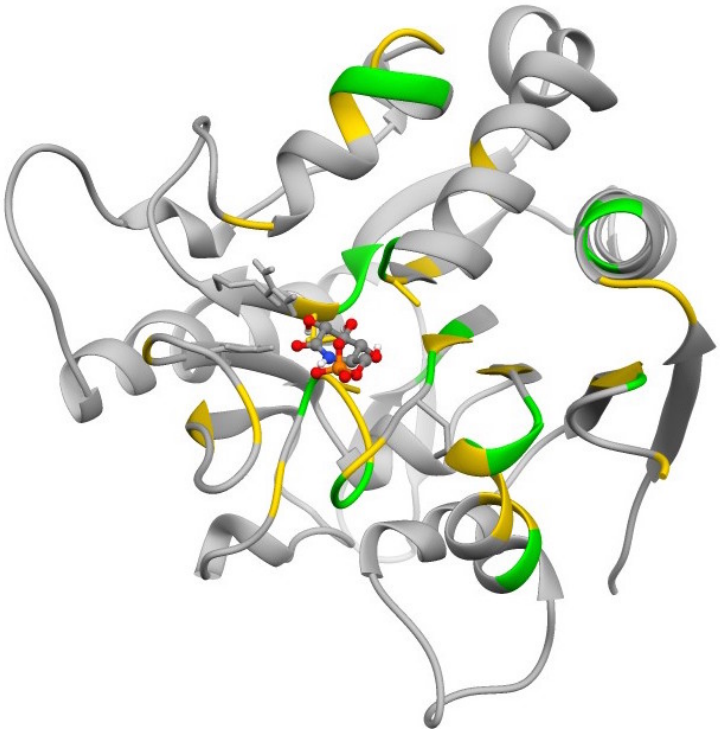

Figure 11: Mapping of the exchanging residues identified by GP269 titration onto the 3D structure of the 6PGL:GP269 complex (CONF1 pose). Residues in fast and intermediate NMR exchange are indicated in yellow and green respectively.